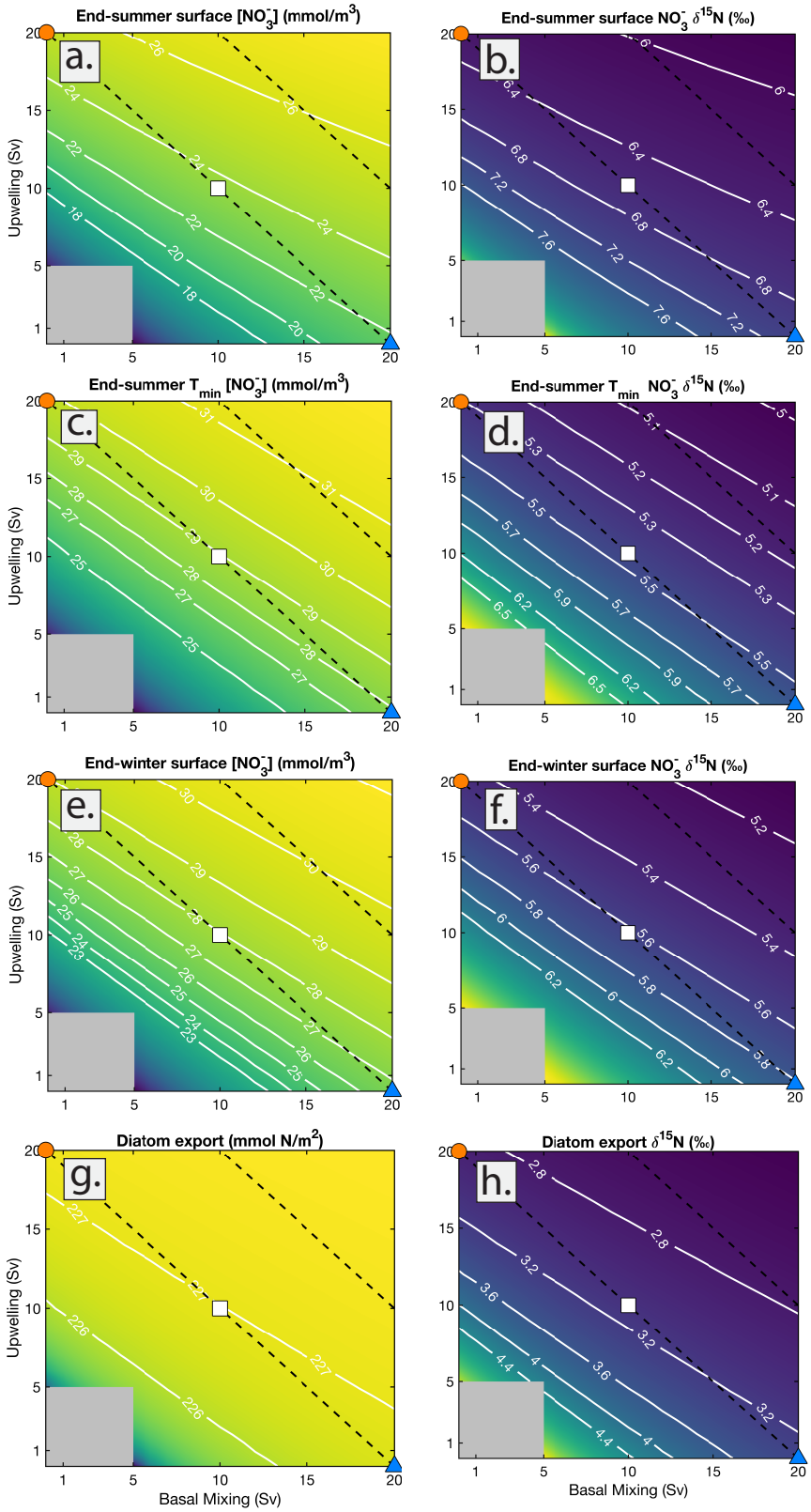

Figure S5: Model results without an active N cycle for moderate magnitudes of upwelling and basal mixing. White squares indicate scenarios discussed in the main text, blue upward triangles and orange circles indicate scenarios plotted in Figure S7.

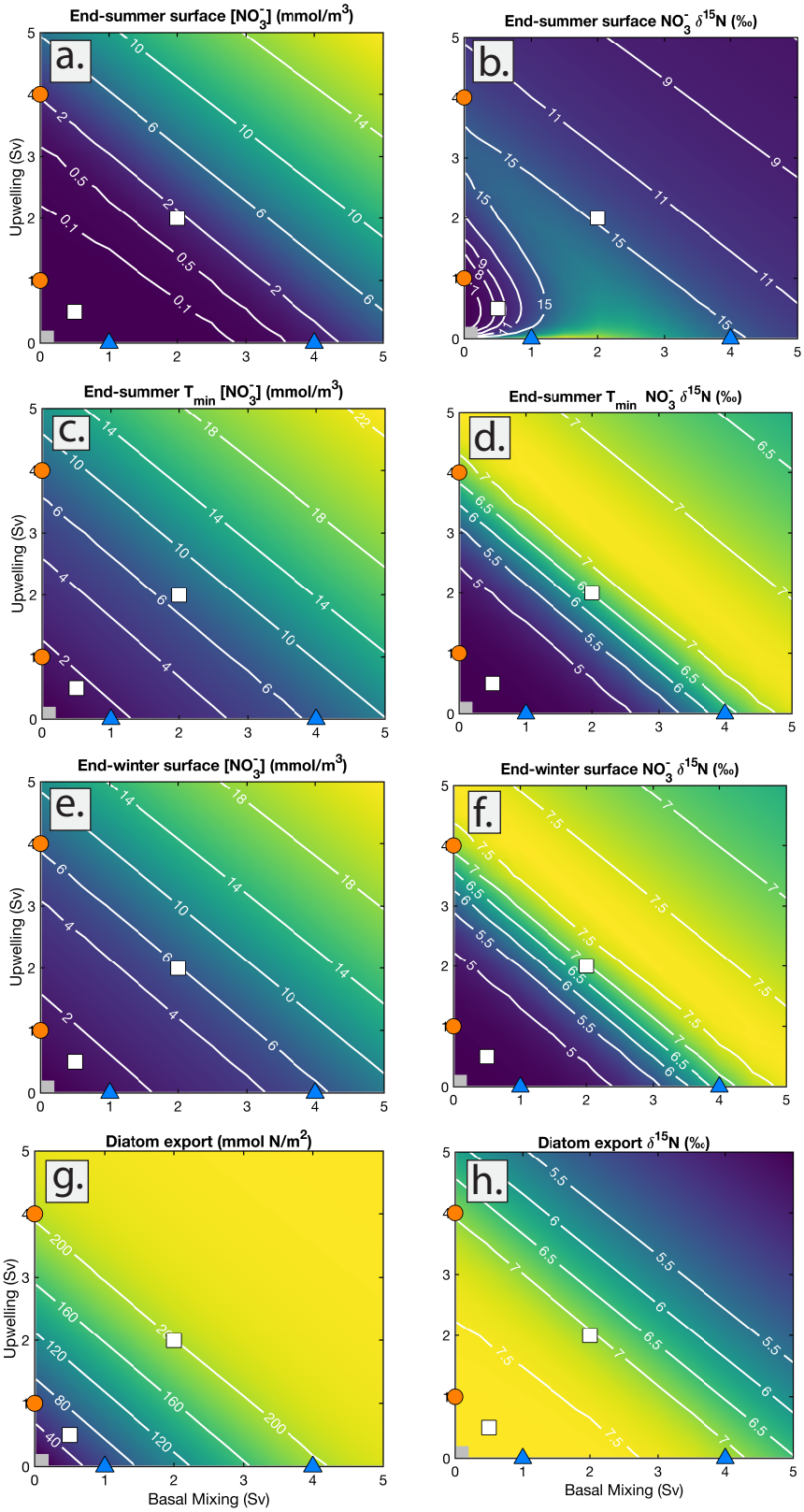

Figure S6: Model results without an active N cycle for low magnitudes of upwelling and basal mixing. White squares indicate scenarios discussed in the main text, blue upward triangles and orange circles indicate scenarios plotted in Figure S7.

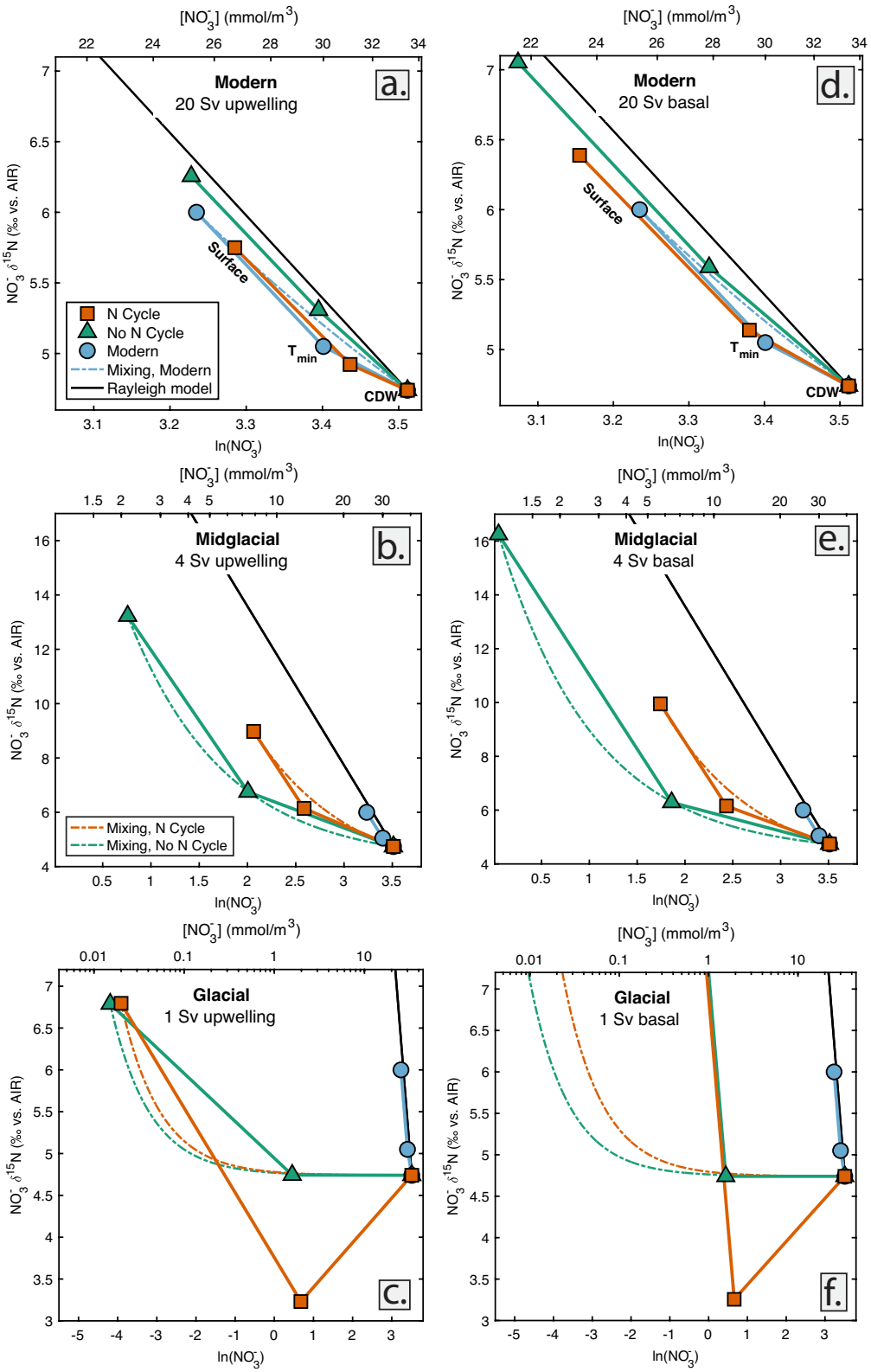

Figure S7: The concentration and $\delta^{15}N$ of NO_3^- in the surface ocean, the T_{min} layer, and CDW for experimental observations (blue circles) and the model with (orange squares) and without (green upward triangles) an active N cycle, for the case of NO_3^- supply exclusively through upwelling (left panels) or basal mixing (right panels).

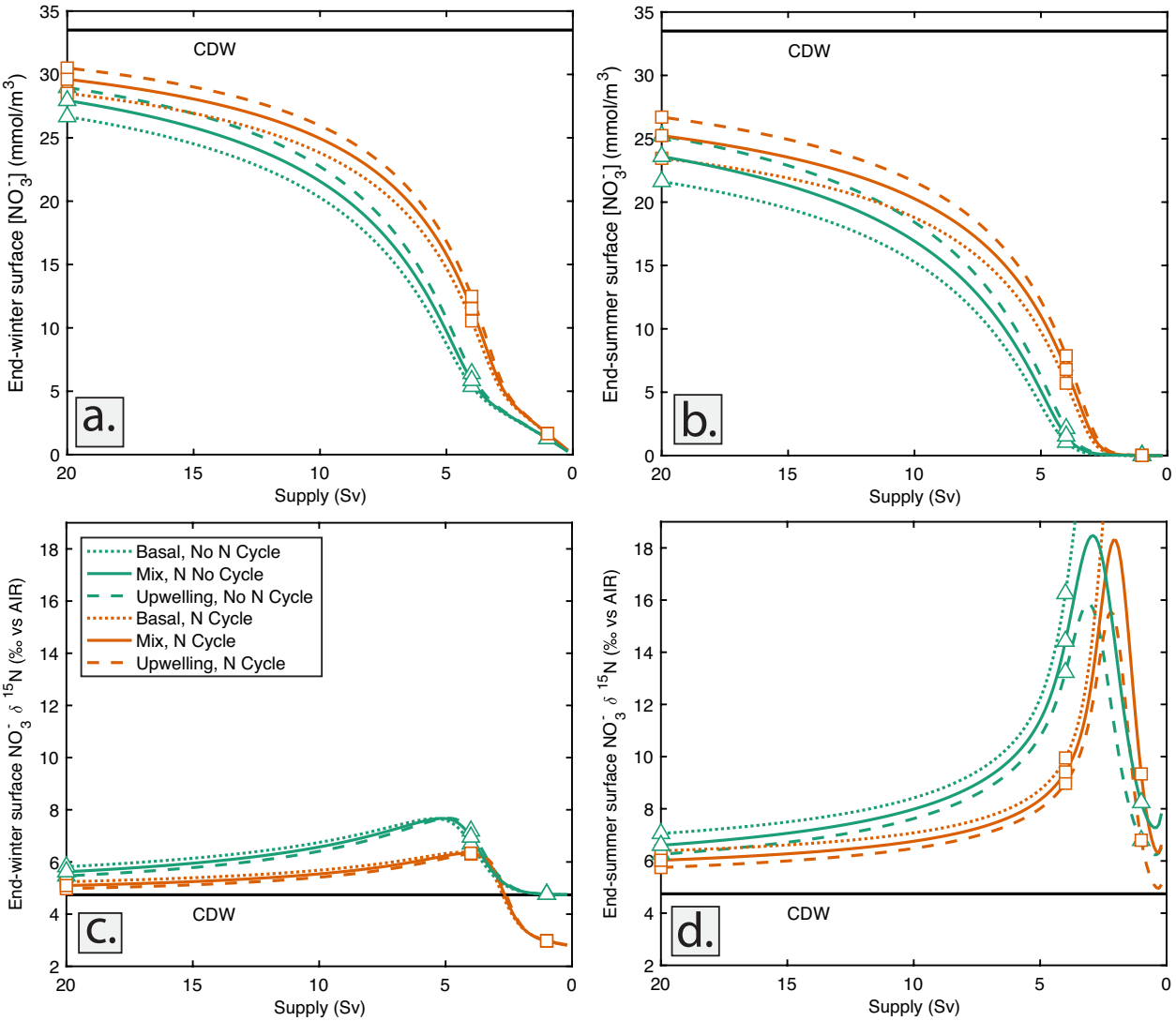

Figure S8: End-winter (**a,c**) and end-summer (**b,d**) surface [NO_3^-] and NO_3^- $\delta^{15}N$ against supply for model results with (orange) and without (green) an active N cycle, starting from the interglacial case of 10 Sv of supply through upwelling and basal mixing (solid), 20 Sv supply through upwelling (dashed), or 20 Sv of supply through basal mixing (dotted). Orange squares and green upward triangles indicate scenarios plotted in Figure S7.

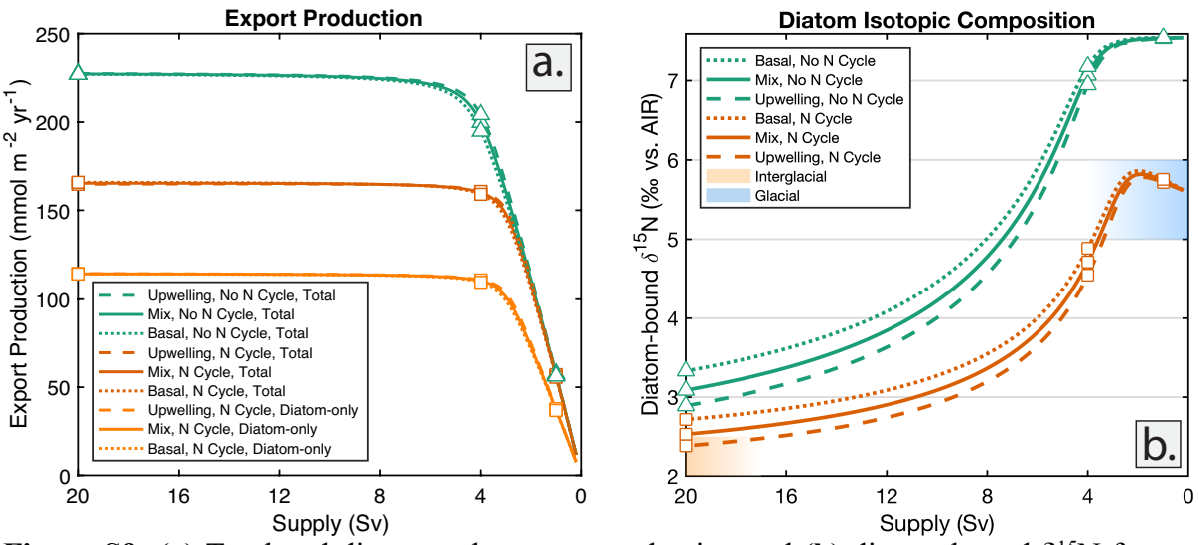

Figure S9: (a) Total and diatom-only export production and **(b)** diatom-bound $\delta^{15}N$ for models with (orange) and without (green) an active N cycle, starting from the interglacial case of 10 Sv of supply through upwelling and basal mixing (solid), 20 Sv supply upwelling (dashed), or 20 Sv of supply through basal mixing (dotted). Orange squares and green upward triangles indicate scenarios plotted in Figure S7.

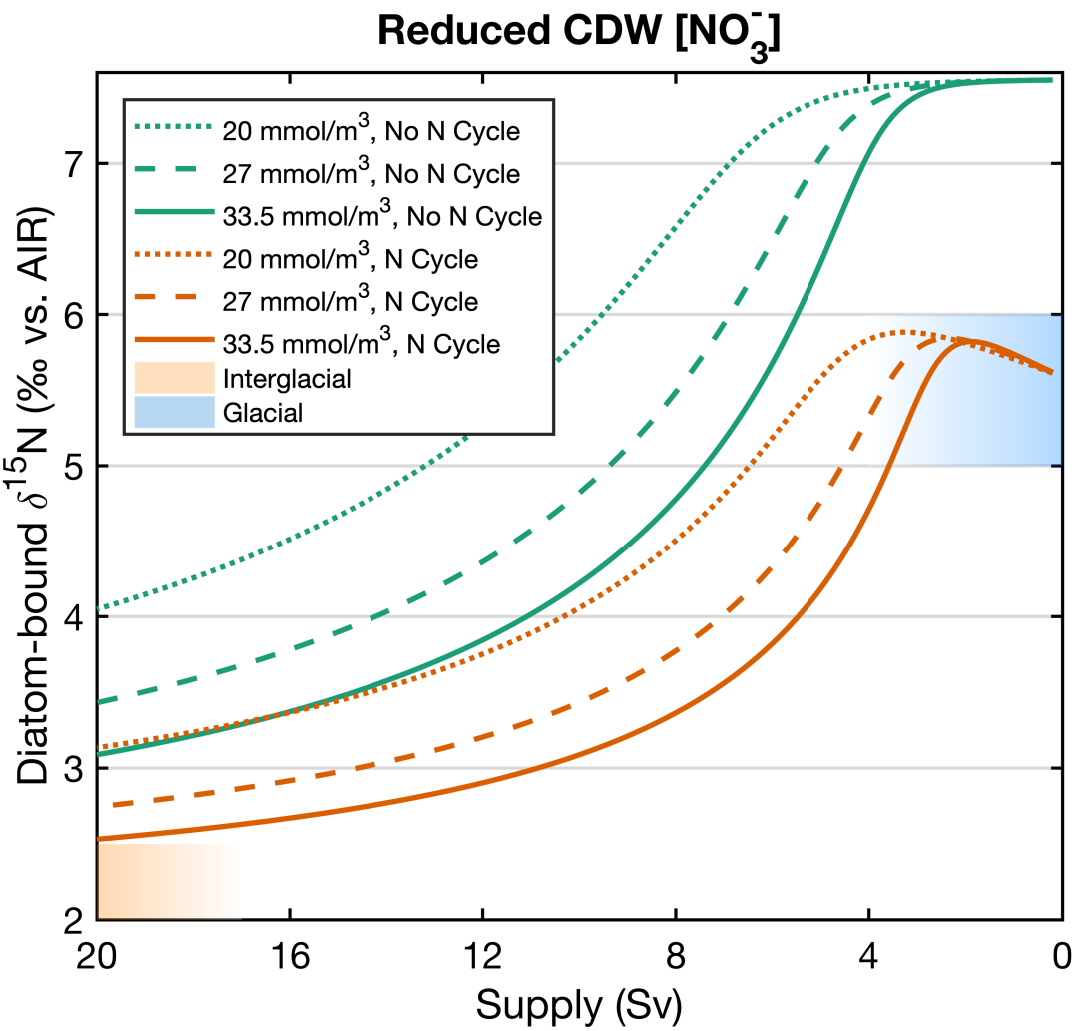

Figure S10: Diatom-bound $\delta^{15}N$ for models with (orange) and without (green) an active N cycle and with CDW [NO_3^-] at 33.5 mmol/m^3 (solid), 27 mmol/m^3 (dashed), or 20 mmol/m^3 (dotted). Reduced CDW [NO_3^-] lowers the required decrease in supply to match observations of $\delta^{15}N_{db}$, but in all cases still requires major reductions in the gross supply of NO_3^-.

Supplement S4: Model sensitivity to changing mixed layer depths

The model simulations reported in the main text have either a constant mixed layer depth of 50 m or a variable summertime mixed layer depth with minimum of 25 m. Here we present additional model results for simulations with variable summertime mixed layer depths. We compare the results from simulations with constant mixed layer depth against those with minimum summertime mixed layer depth of either 25 m or 10 m (Figures S11, S12, and S13). The choice of model parameters is the same as in the main text, which were calibrated to modern observations for the use of 10 Sv upwelling and 10 Sv of basal mixing. The major impact of shoaling the summertime mixed layer is that a given addition of CDW, either through upwelling or basal mixing, becomes a volumetrically larger fraction of the surface ocean. At a given magnitude of water supply, surface [NO_3^-] and NO_3^- $\delta^{15}N$ will thus be more strongly drawn towards the values of CDW in simulations with variable mixed layer depth than in simulations with a deeper mixed layer (Figure S12). As a result, reaching the observed ~3-4‰ increase in diatom-bound $\delta^{15}N$ require an even larger reduction in the gross NO_3^- supply beyond that calculated for a constant, deeper mixed layer (Figure S13).

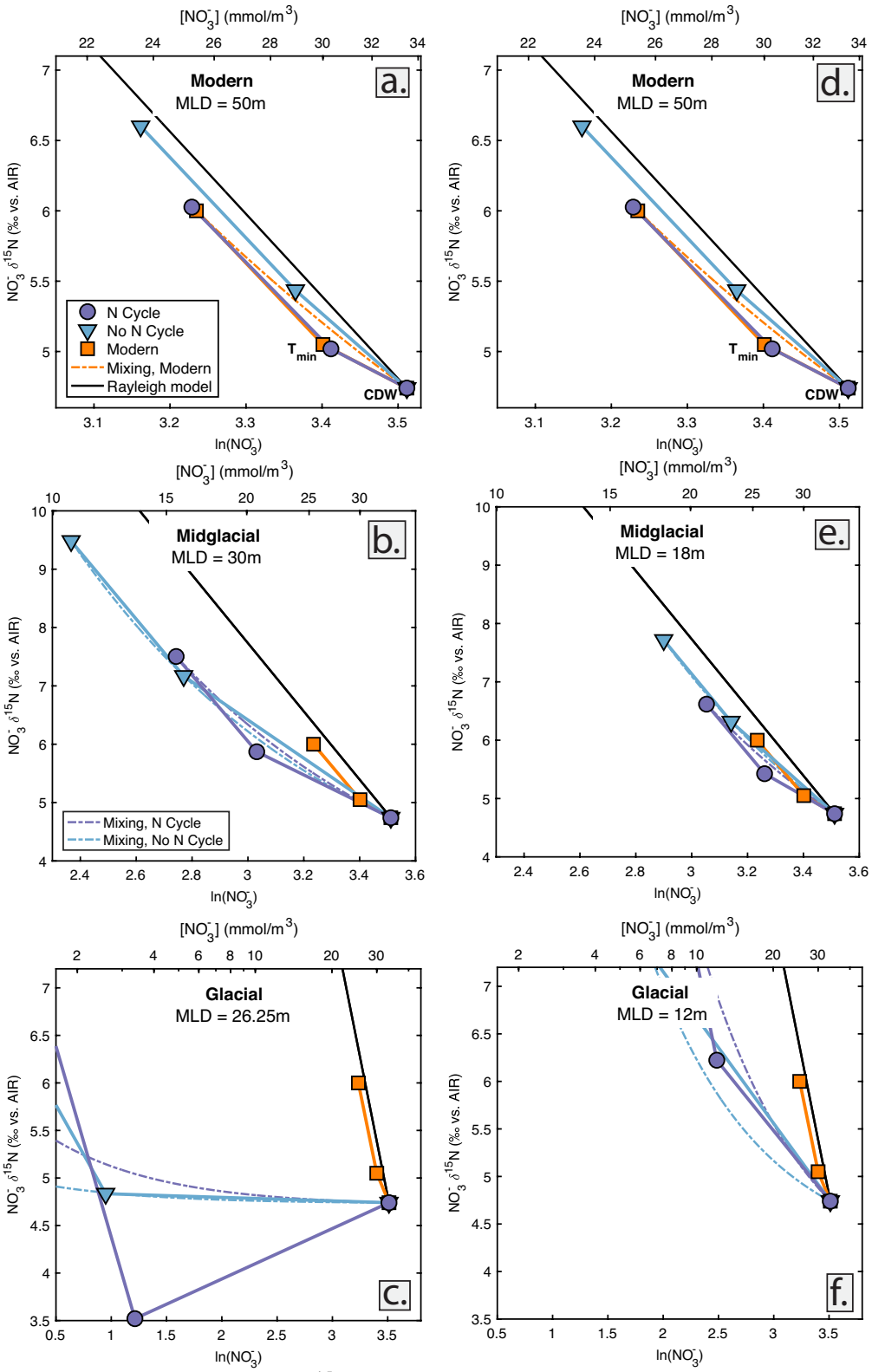

Figure S11: The concentration and $\delta^{15}N$ of NO_3^- in the surface ocean, the T_{min} layer, and CDW for experimental observations (orange squares) and the model with (purple circles) and without (blue downward triangles) an active N cycle, for variable summertime mixed layer depths with minimum of 25 m (left panels), or minimum of 10 m (right panels).

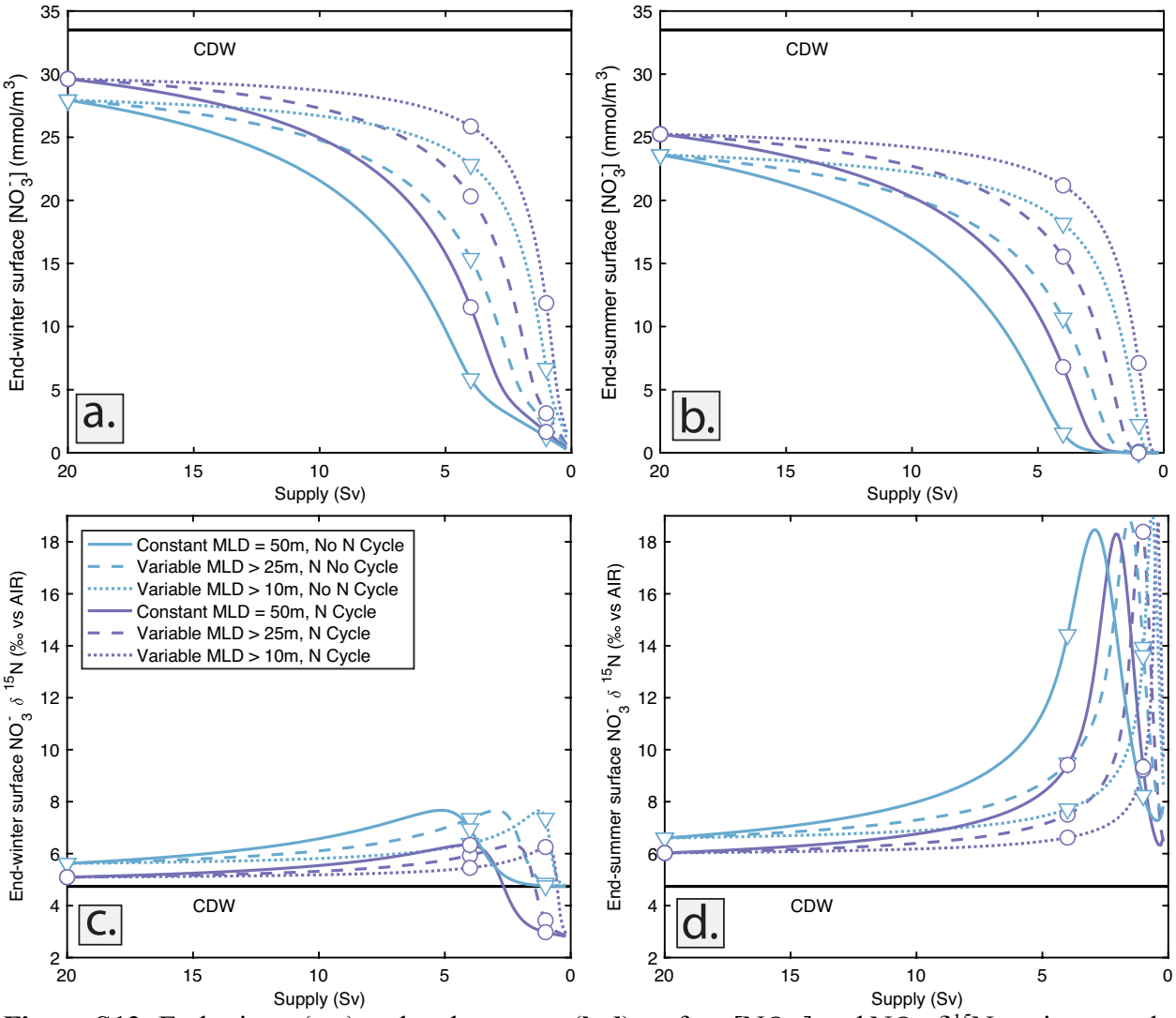

Figure S12: End-winter (**a,c**) and end-summer (**b,d**) surface [NO_3^-] and NO_3^- $\delta^{15}N$ against supply for model results with (purple) and without (blue) an active N cycle, for models with a constant mixed layer depth (solid), variable summertime mixed layer depth with minimum of 25 m (dashed), or variable summertime mixed depth with minimum of 10 m (dotted). Purple circles and blue downward triangles indicate scenarios plotted in Figure S11.

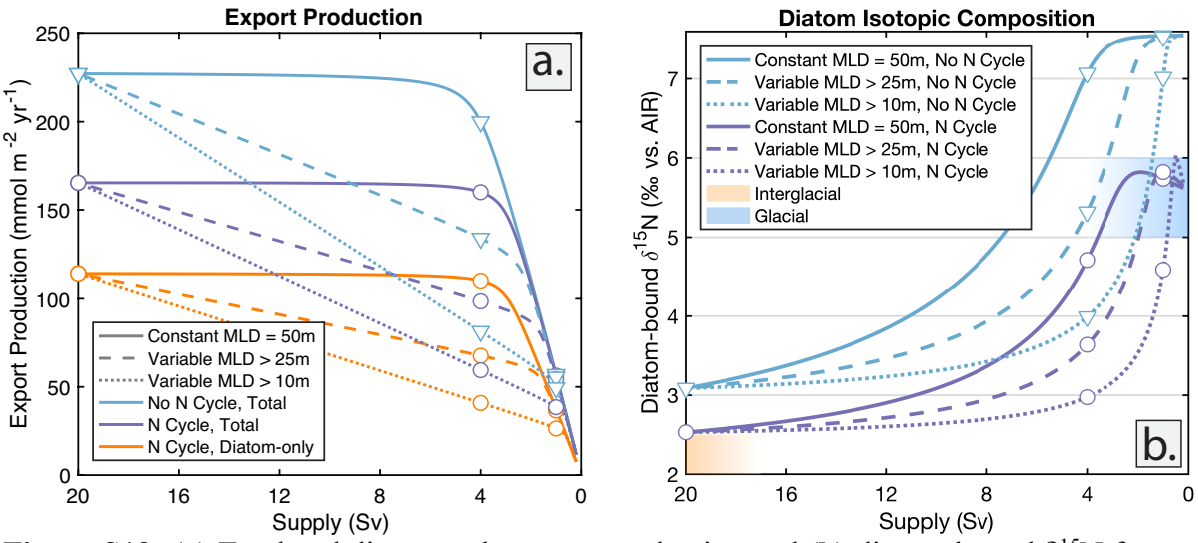

Figure S13: (a) Total and diatom-only export production and **(b)** diatom-bound $\delta^{15}N$ for models with (orange) and without (green) a N cycle, for models with a constant mixed layer depth (solid), variable summertime mixed layer depth with minimum of 25 m (dashed), or variable summertime mixed depth with minimum of 10 m (dotted). Purple circles and blue downward triangles indicate scenarios plotted in Figure S11.

Supplement S5: Origin of the modern T_{min} kink

The origins of and controls on the NO_3^- initially available for spring/summer assimilation in the AZ have been investigated using depth profiles of $[NO_3^-]$ and NO_3^- $\delta^{15}N$ from the OAZ and PAZ, the northern and southern regions of the AZ. These two Antarctic zones show differences in the relationship of NO_3^- $\delta^{15}N$ to $[NO_3^-]$ (DiFiore et al., 2010). Summertime PAZ NO_3^- $\delta^{15}N$ increases linearly as $\ln([NO_3^-])$ decreases due to NO_3^- assimilation, with the relationship among deep water, the winter mixed layer, and the summer mixed layer in accordance with the Rayleigh model (DiFiore et al., 2009). However, summertime profiles from the OAZ show a deviation in the T_{min} layer where the $\delta^{15}N$ of NO_3^- is lower than expected for its concentration. This offset between measured and expected $\delta^{15}N$ is referred to as the "kink" of the T_{min} layer and represents an underexpression of the NO_3^- assimilation isotope effect, relative to the predictions of the Rayleigh model, over the vertical extent of the winter mixed layer (Sigman et al., 1999; DiFiore et al., 2010; Smart et al., 2015; Kemeny et al., 2016). With the Rayleigh model limited to a single closed reservoir, this simple framework cannot explain the kink and strongly suggests that a more complex model should be used for understanding nitrogen cycling in the modern and glacial AZ. In the modern AZ, the isotopic kink is a relatively subtle feature, reflecting a deviation of only 0.2-0.5‰ in the $\delta^{15}N$ of T_{min} NO_3^- relative to Rayleigh model predictions. Nevertheless, it may have important implications for the seasonal supply of NO_3^- to the AZ surface ocean and thus for interpreting paleoceanographic proxies in a seasonal context. Moreover, as with the assumptions inherent in the Rayleigh model, the kink may be more significant under the higher degree of NO_3^- consumption inferred for the ice age AZ.

Four explanations for the origin of the isotopic kink in the T_{min} layer are briefly summarized below, and they bear strongly on understanding the formation of the T_{min} layer itself: (1) seasonal

mixing of the surface and CDW (Sigman et al., 1999), (2) lateral exchange of the T_{min} (DiFiore et al., 2009, 2010), (3) late summer N cycling and wintertime nitrification (Smart et al., 2015), and (4) fractionation during the remineralization of sinking organic matter. In general, the seasonally varying vertical structure of the AZ, of which the summertime kink is a consequence, should be considered in the broader effort to interpret high latitude proxies for upper ocean biogeochemistry in the past. The model approximately simulates the modern T_{min} kink in the relationship between $\ln([NO_3^-])$ and NO_3^- $\delta^{15}N$ (Figure 4a).

The first proposed explanation for the T_{min} isotopic kink is that it reflects a long-term mixture between deep water and shallow surface water. In mixing of waters from the surface mixed layer (with lower $[NO_3^-]$) and CDW (with higher $[NO_3^-]$) the $[NO_3^-]$ of the mixture will be a volume-weighted average of the mixing end-members while the NO_3^- $\delta^{15}N$ is also weighted by the $[NO_3^-]$ of the mixing reservoirs. This dynamic will bring the NO_3^- $\delta^{15}N$ of the mixture closer to CDW and thus generate a $\delta^{15}N$ kink of the same sense that is observed in the T_{min}. However, the low degree of nutrient consumption in the modern AZ surface prevents mixing from generating a signal of sufficient magnitude to explain the T_{min} feature (Sigman et al., 1999). Under scenarios of more complete NO_3^- consumption, such as those that likely characterize ice ages (Studer et al., 2015), mixing may have had a greater capacity to drive deviations from Rayleigh expectations. In the modern Antarctic, the model confirms that the $[NO_3^-]$ differences between the summer surface and CDW are too low for seasonal or longer-term mixing to generate the observed amplitude of the T_{min} $\delta^{15}N$ kink (Figure 4a, dotted mixing line) (see also Sigman et al., 1999). However, in the space of $\delta^{15}N$ vs. $\log([NO_3^-])$, long-term mixing does generate a lower slope than the Rayleigh model predicts even in the absence of summertime N recycling (Figure 4a, 'No N Cycle'). This observation shows that seasonal mixing generates a deviation from Rayleigh expectations even in

the modern AZ, although not to a degree that can explain the modern T_{min} isotopic kink. A much stronger kink develops as a result of this mixing dynamic during ice age simulations with reduced NO_3^- supply (Figure 4b, 4c, dotted mixing lines). That is, under inferred glacial conditions the relationship between NO_3^- concentration and $\delta^{15}N$ deviates substantially from Rayleigh model behavior even in the absence of internal N cycling, with significant consequences for the interpretation of ice age $\delta^{15}N$ records.

A second explanation for the isotopic kink is that it results from lateral mixing between the T_{min} and other water masses. The coastal PAZ has been observed to have a mid-depth maximum in temperature with the same potential density as the T_{min} layer (DiFiore et al., 2009). Previously, lateral exchange between this layer and the T_{min} was proposed to explain the isotopic kink by mixing waters sourced from Lower Circumpolar Deep Water (LCDW) into intermediate depths above Upper Circumpolar Deep Water (UCDW) (DiFiore et al., 2010). However, this explanation has been cast into doubt by observations of a T_{min} isotopic kink in profiles underlain by LCDW (Smart et al., 2015; Kemeny et al., 2016).

Third, the upper ocean N cycle has been shown to be a likely contributor to the kink in the Southern Ocean Atlantic Sector (Smart et al., 2015). Lourey et al. (2003) report that the $\delta^{15}N$ of surface suspended particulate nitrogen (PN) in the PFZ decreases from ~1‰ to ~-5‰ during the summer, interpreted to result from late summer N recycling in which heterotrophs release low-$\delta^{15}N$ NH_4^+ into the environment (Koike et al., 1986; Checkley & Miller, 1989). Smart et al. (2015) showed that measurements of winter NO_3^- $\delta^{15}N$ are consistent with wintertime nitrification of the low-$\delta^{15}N$ PN inherited from the prior summer and fall. In turn, the addition of this material to the water column can generate an offset from Rayleigh expectations that survives into the following summer. In the modern scenario, our modeling shows that the kink results dominantly from the

wintertime remineralization of low-$\delta^{15}N$ PN in the combined surface and T_{min} layers, consistent with the explanation for this feature proposed by Smart et al. (2015). PN becomes low in $\delta^{15}N$ due to intensive N cycling in the end-summer surface ocean (Figure 3). In turn, the lowering of NO_3^- $\delta^{15}N$ in the winter mixed layer by the remineralization and nitrification of this PN lowers the $\delta^{15}N$ of the summertime NO_3^- pool available for the summer diatom bloom, decreasing slightly the $\delta^{15}N$ of diatom biomass that is produced over the summer. In the model's interglacial scenario (Figure 4a), the recycling of regenerated N in the mixed layer depresses end-summer NO_3^- $\delta^{15}N$ in the T_{min} layer by 0.42‰ relative to the model without an active N cycle, which is a modest effect. However, as with the effect of mixing, the isotopic impact of N recycling increases at lower rates of NO_3^- supply from below and thus intensifies in the simulations of glacial separation (Figure 4b, 4c; the difference between the no N cycling and active N cycling cases).

Lastly, an alternative process that may contribute to the T_{min} isotopic kink is fractionation associated with the remineralization of sinking organic matter. In one scenario for this process, sinking particles exported from the surface ocean that are disaggregated in the T_{min} layer undergo remineralization with isotope fractionation, consistent with observations for deep ocean suspended PN $\delta^{15}N$ (Altabet et al., 1991). The remaining suspended PN would thus be elevated in $\delta^{15}N$. If this PN is repackaged by zooplankton in the T_{min}, producing new sinking particles, then the net result would be to retain low-$\delta^{15}N$ N in the upper water column of the AZ. This effect is similar to that from N cycling within the summertime AZ in that both generate the T_{min} kink by preferentially exporting high-$\delta^{15}N$ N and retaining low-$\delta^{15}N$ N for subsequent nitrification in the T_{min} or winter mixed layer. These two scenarios could be distinguished by comparing the $\delta^{15}N$ of N exported from the surface mixed layer and from the base of the T_{min} layer, or through a time-series analysis of the summertime evolution of the T_{min} layer, both of which will require new measurements. As

discussed, our primary results do not include isotope fractionation in the remineralization of sinking PN as it passes through the T_{min}. This exclusion may cause our parameter fitting to overestimate the role of N recycling in the summer mixed layer followed by wintertime nitrification in generating the deviations from Rayleigh predictions in the modern AZ. To explore this hypothesis, we briefly present two scenarios. Scenario 1 is the model discussed in the main text, where the isotopic kink of the modern T_{min} layer is principally derived from the wintertime nitrification of low-$\delta^{15}N$ PN. In scenario 2, we increase the remineralization fraction from 10% to 20%, alter the isotope effect of remineralization from 0‰ to -3‰ (favoring the retention of ^{14}N in the upper ocean), and decrease the rate of diatom consumption by zooplankton from 3% per day to 1% per day (Table S1). Note that all other parameters are unchanged from their values in the main text (Table 1), and that N bound within diatom frustules remains protected from remineralization in both scenarios. The seasonal changes in seawater [NO_3^-] and NO_3^- $\delta^{15}N$ are quite similar in the two scenarios (Table S2, Figure S14a), suggesting that remineralization with isotopic fractionation is a viable explanation for the formation of the modern T_{min} isotopic kink. Moreover, the model predicts similar ice age diatom-bound $\delta^{15}N$ values for both scenarios, implying comparable predictions for the ice age reduction in the gross supply of NO_3^- (Figure S14b). However, the second scenario has significantly lower abundances for all biological N reservoirs except diatoms (Table S2), suggesting that the two scenarios could be distinguished through seasonal studies of the individual biomass pools contributing to total PN.

Model Parameter	**Scenario 1: Recycling**	**Scenario 2: Remineralization**
Export remineralization	10%	20%
Remineralization fractionation	0‰	-3‰
Zoo. diatom uptake	3%/day	1%/day

Table S1: Model parameters that differ for the two scenarios plotted below. All other parameters equal their values in Table 1 of the main text.

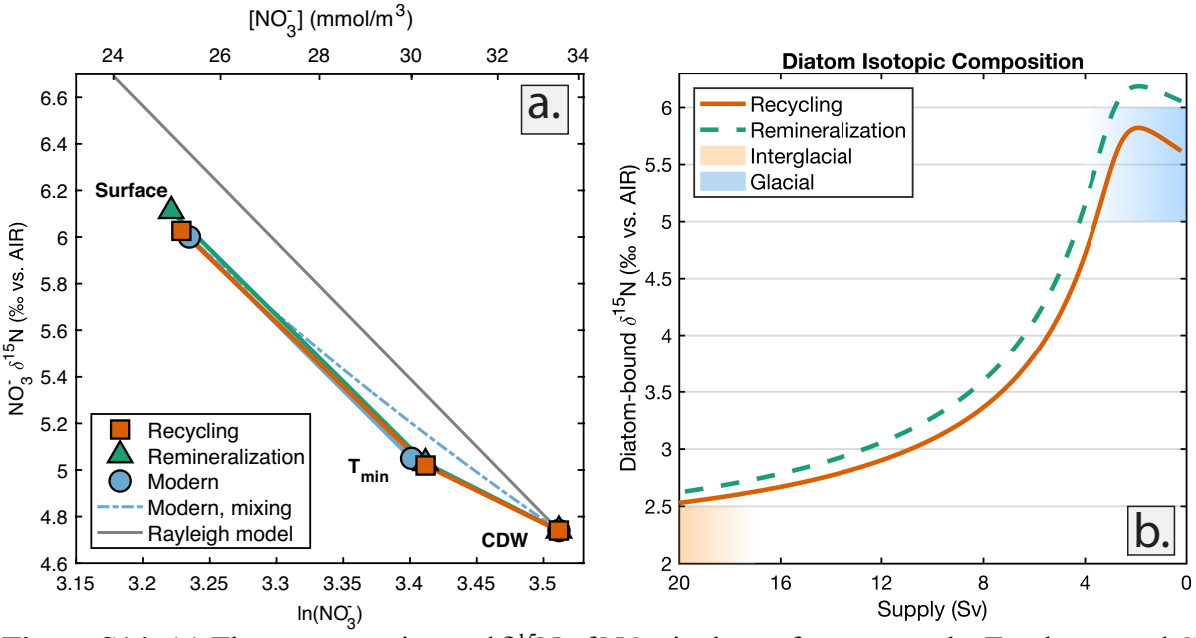

Figure S14: (a) The concentration and $\delta^{15}N$ of NO_3^- in the surface ocean, the T_{min} layer, and CDW for modern observations (blue circles), a system dominated by N recycling (orange squares), and a system with fractionation during remineralization (green upward triangles), for 10 Sv of NO_3^- supply through upwelling and 10 Sv through basal mixing. **(b)** Diatom-bound $\delta^{15}N$ for scenarios dominated by N recycling (solid orange) or with fractionation during remineralization of exported PN in the T_{min} layer (dashed green).

Modern Observation	**Scenario 1: Recycling**	**Scenario 2: Remineralization**	**Observed**
End-summer Srf $[NO_3^-]$ (mmol/m^3)	25.25	25.06	25.4
End-summer Srf NO_3^- $\delta^{15}N$ (‰)	6.03	6.11	6.0
End-summer T_{min} $[NO_3^-]$ (mmol/m^3)	30.32	30.31	30.0
End-summer T_{min} NO_3^- $\delta^{15}N$ (‰)	5.02	5.03	5.05
Max. summer diatom (mmol/m^3)	0.93	1.36	0.75-1.00
Max. summer zooplankton (mmol/m^3)	0.34	0.16	0.25-0.50
Max. summer non-diatom (mmol/m^3)	0.97	0.47	0.75-1.00
Max. summer $[NH_4^+]$ (mmol/m^3)	0.49	0.23	0.30-0.70 0.50-1.50
Max. winter $[NH_4^+]$ (mmol/m^3)	0.72	0.37	-
End-summer PN (mmol/m^3)	1.00	0.55	0.50-1.00 *varied*
End-summer suspended PN $\delta^{15}N$ (‰)	-5.08	-4.31	~ -5.0
Total export production (mmol/m^2)	165.3	173.5	100-500
Diatom/zooplankton export ratio	2.21	6.95	~2

Table S2: Comparison of observations and model results under two different sets of parameters. References for observed values are given in Table 2 of the main text.